Available at www.sciencedirect.com

ScienceDirect

journal homepage: www.elsevier.com/locate/he

Thermo-electrochemical modeling of ammonia-fueled solid oxide fuel cells considering ammonia thermal decomposition in the anode

*Meng Ni**

Department of Building and Real Estate, The Hong Kong Polytechnic University, Hung Hom, Kowloon, Hong Kong

ARTICLE INFO

Article history:
Received 11 September 2010
Received in revised form
18 November 2010
Accepted 25 November 2010
Available online 30 December 2010

Keywords:
Solid oxide fuel cells
Heat transfer
Electrochemistry
Porous media
Ammonia thermal decomposition

ABSTRACT

Ammonia (NH_3) is a promising hydrogen carrier and a possible fuel for use in Solid Oxide Fuel Cells (SOFCs). In this study, a 2D thermo-electrochemical model is developed to investigate the heat/mass transfer, chemical (ammonia thermal decomposition) and electrochemical reactions in a planar SOFC running on ammonia. The model integrates three sub-models: (1) an electrochemical model relating the current density–voltage characteristics; (2) a chemical model calculating the rate of ammonia thermal decomposition reaction; (3) a 2D computational fluid dynamics (CFD) model that simulates the heat and mass transfer phenomena. Simulations are conducted to study the complicated physical–chemical processes in NH_3-fueled SOFCs. It is found that increasing the inlet temperature of NH_3-fueled SOFC is favorable for a higher electric output, but the temperature gradient in the SOFC is considerably higher, particularly near the inlet of the SOFC. The effects of operating potential and inlet gas velocity on NH_3-fueled SOFC performance are investigated. It is found that an increase in inlet gas velocity from 1 m s^{-1} to 10 m s^{-1} slightly decreases the SOFC performance and does not affect the temperature field significantly. For comparison, decreasing the gas velocity to 0.2 m s^{-1} is more effective to reduce the temperature gradient in SOFC.

1. Introduction

Solid oxide fuel cells (SOFCs) are electrochemical devices that can directly convert the chemical energy of a fuel into electricity through electrochemical reactions. Working at a high temperature (673–1273 K), SOFCs have several advantages: (1) possibility of using low cost catalyst, such as Ni at the anode; (2) the waste heat from SOFC is of high quality and can be recovered to achieve a high efficiency [1–3]; (3) fuel flexibility – alternative fuels such as hydrocarbon fuels and ammonia, can be directly used in an SOFC for power generation [4–6]. As a result, SOFCs are suitable for combined heat and power (CHP) generation or poly-generation for stationary applications.

Conventional SOFCs use oxygen ion-conducting ceramics as electrolyte (SOFC-O) [7,8]. Recent material developments demonstrated that an SOFC can also be made with a proton-conducting electrolyte (SOFC-H) [9]. Thermodynamic analysis has shown that an SOFC-H has potentially higher performance than SOFC-O due to higher Nernst potential of SOFC-H. But currently, the actual performance of SOFC-H is still lower than SOFC-O, due to higher ohmic overpotential of the proton-conducting electrolyte [10].

* Tel.: +852 2766 4152; fax: +852 2764 5131.
E-mail addresses: memni@graduate.hku.hk, bsmengni@polyu.edu.hk.
0360-3199/$ – see front matter © 2010 Professor T. Nejat Veziroglu. Published by Elsevier Ltd. All rights reserved.
doi:10.1016/j.ijhydene.2010.11.100

Although hydrogen (H_2) is usually considered as an ideal fuel for fuel cells and the performance of H_2-fueled fuel cells is quite good, it is still very difficult to produce and store H_2 efficiently and economically. It is therefore important to use alternative fuels in SOFCs, such as biofuels and ammonia. Ammonia is a widely used material in chemical industry. For example, it is widely used as a chemical in agricultural industry. The infrastructure of ammonia is well established in the world. Its production, storage, transportation are well developed. In addition, ammonia is relatively safe for use, as any leakage of ammonia can be easily detected by its odor. Thus, there is increasing interest in using ammonia as a hydrogen carrier and a suitable fuel for SOFCs [11,12].

In the literature, there are plenty of experimental studies on ammonia-fueled SOFCs. These studies not only demonstrated the technical feasibility of using ammonia as a fuel in SOFCs, but also proved that the SOFC performance can be enhanced by developing new materials or fabricating thin film electrolyte. In addition to experimental investigation, the SOFC performance can also be improved by optimizing the working conditions or optimizing the fuel cell structures. For example, one can optimize the flow field of SOFC stack to increase the stack efficiency, or optimize the electrode micro-structure to improve the SOFC performance. In order to achieve design optimization, a deep understanding of the complicated physical–chemical processes in SOFC is essential. Although there are lots of modeling studies of SOFCs running on hydrogen or natural gas [13–23], the results obtained cannot be directly applied to NH_3-fueled SOFCs. In a NH_3-fueled SOFC, endothermic ammonia thermal decomposition may considerably influence the temperature field of the SOFC and thus can affect the transport process of gas species as well as the electric output of SOFCs. In a previous study, one-dimensional electrochemical models have been developed for a NH_3-fueled SOFC [10]. Through model validation and parametric simulation, the model has been demonstrated to be useful in estimating the current density–voltage relationship of a NH_3-fueled SOFC. However, in the one-dimensional model, only mass transfer and electrochemical reactions thus it could not provide detailed information on the heat/mass transfer and chemical/electrochemical reactions in the NH_3-fueled SOFC. In this study, a two-dimensional thermo-electrochemical model is developed by integrating a computational fluid dynamics model with an electrochemical model and a chemical model to simulate NH_3-fueled SOFCs [24,25]. The mass transfer, heat transfer, chemical reaction (ammonia thermal decomposition) and electrochemical reaction are fully considered. Parametric simulations are conducted with an aim to understand how the inclusion of ammonia thermal decomposition will affect the SOFC performance.

2. Model development

In this study, ammonia is directly used as a fuel in SOFCs. The computation domain and the chemical/electrochemical reactions are shown in Fig. 1. The key geometric dimensions are summarized in Table 1.

During operation, ammonia and air are fed to the anode channel and cathode channel, respectively. In the porous cathode, oxygen molecules are transported to the cathode–electrolyte interface, where oxygen molecules react with electrons to produce oxygen ions, which are subsequently transported through the dense electrolyte to the porous anode. In the porous anode, ammonia is thermally decomposed into hydrogen and nitrogen (Eq. (1)). The hydrogen molecules are diffused through the anode to the anode–electrolyte interface, where hydrogen molecules react with oxygen ions to produce steam and electrons. The electrochemically produced electrons are collected by the current collector (interconnect) and then transported to the cathode through the external circuit to complete the cycle. The overall electrochemical reaction can be written in Eq. (2).

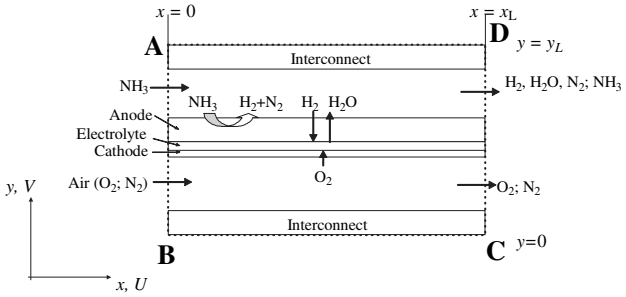

Fig. 1 – Computational domain of NH_3-fueled SOFC; thickness of interconnector: 0.5 mm; height of the fuel/air channel: 1.0 mm; thickness of porous anode, electrolyte, and porous cathode are: 0.5 mm, 0.1 mm and 0.1 mm, respectively.

$$NH_3 \rightarrow 1.5H_2 + 0.5N_2 \quad (1)$$

$$H_2 + 0.5O_2 \rightarrow H_2O \quad (2)$$

Table 1 – Parameters used in simulation [24].

Parameter	Value
Inlet temperature, T (K)	873
Operating pressure, P (bar)	1.0
Electrode porosity, ε	0.4
Electrode tortuosity, ξ	3.0
Average pore radius, r_p (μm)	0.5
Anode-supported electrolyte:	
Anode thickness d_a (μm)	500
Electrolyte thickness, d_e (μm)	100
Cathode thickness, d_c (μm)	100
Height of gas flow channel, H_F (mm)	1.0
Length of the planar SOFC, L (mm)	20
Thickness of interconnect (mm)	0.5
Inlet velocity: U_{in} (m s^{-1})	1.0
Cathode inlet gas molar ratio: O_2/N_2	0.21/0.79
Anode inlet gas:	100% NH_3
SOFC operating potential (V)	0.8
Thermal conductivity of SOFC component (W m^{-1} K^{-1})	
Anode	11.0
Electrolyte	2.7
Cathode	6.0
Interconnect	1.1

Based on the working mechanisms, a 2D thermo-electrochemical model is developed by integrating an electrochemical model and a chemical model with a 2D CFD model. The details of the three sub-models are described in the subsequent sections.

2.1. Electrochemical model

The electrochemical model is built to describe the current density–voltage relationship of SOFCs. A planar SOFC with oxygen ion-conducting electrolyte is considered. The typical materials for SOFC are nickel, yttria-stabilized zirconia (Ni–YSZ) anode, yttria-stabilized zirconia (YSZ) electrolyte, and yttria-stabilized zirconia, lanthanum strontium manganite (YSZ–LSM) cathode. It is assumed that only hydrogen and oxygen are involved in the electrochemical reaction and electrochemical oxidation of ammonia is neglected. Along the SOFC channel, the interconnector is used to collect current produced. As the electrical conductivity of interconnector is high, it can be safely assumed that the potential of SOFCs along the main flow stream remains constant. Therefore, the electrochemical model is used to calculate the local current density at given operating potentials. During operation, the relationship between current density (J) and electrochemical potential (V) of an SOFC can be obtained by solving the following equations [25],

$$V = E - \eta_{act,a} - \eta_{act,c} - \eta_{ohmic} \tag{3}$$

$$E = E_0 + \frac{RT}{2F}\ln\left[\frac{P^I_{H_2}\left(P^I_{O_2}\right)^{0.5}}{P^I_{H_2O}}\right] \tag{4}$$

$$E_0 = 1.253 - 0.00024516T \tag{5}$$

where E is the equilibrium potential and E_0 is the equilibrium potential at standard pressure; T is the local temperature (K); η_{ohmic} is the ohmic overpotential of the electrolyte; $\eta_{act,a}$ and $\eta_{act,c}$ are the activation overpotentials at the anode and cathode, respectively; P^I is the partial pressure at the electrode–electrolyte interface; R is the universal gas constant (8.3145 J mol^{-1} K^{-1}); and F is the Faraday constant (96485 C mol^{-1}). It should be mentioned that the concentration overpotentials are included in the Nernst potential (E), since the partial pressures of gaseous species in Eq. (4) are evaluated at the electrode–electrolyte interface. The reason to include the concentration overpotentials in the Nernst potential (Eq. (4)) is because the logarithm in the Nernst potential could be mathematically incorrect with a hydrogen partial pressure of zero at the anode surface. By including the concentration overpotentials in the Nernst potential, this problem can be solved, as the partial pressure of hydrogen is non-zero at the anode–electrolyte interface due to NH_3 decomposition. The ohmic and activation overpotentials can be calculated with Ohm's law and Butler–Volmer equations, respectively [25].

2.2. Chemical model – thermal decomposition of ammonia in anode

As ammonia is directly used as a fuel, the hydrogen molar fraction at the inlet is zero. At the inlet of SOFC, the molar fraction of NH_3 0.9999 is used with the H_2 fuel, H_2O and N_2 as trace gases to approximate pure NH_3 at the inlet. The thermal decomposition of ammonia for hydrogen production in the porous anode is solved through the chemical model described in this section. It should be mentioned that NH_3 thermal decomposition could take place in the anode (fuel) channel, as this process is favored at high temperature. According to thermodynamics, at a temperature of 1273 K, the equilibrium conversion of NH_3 could be close to 100%. However, this process is slow with no catalyst [11] and that's why substantial research efforts have been made to develop efficient catalyst for NH_3 catalytic thermal decomposition. Even with effective catalyst (Ni–Pt or Ru), the conversion of NH_3 into H_2 and N_2 is still considerably lower than the conversion based on thermodynamic equilibrium [26]. Other studies also shown that the rate of NH_3 thermal decomposition (with no catalyst) is considerably lower than NH_3 catalytic thermal decomposition [27]. Therefore, in the present study, the decomposition of NH_3 without catalyst is assumed to be negligible and only catalytic thermal decomposition of NH_3 in the porous anode layer is considered. Nevertheless, the present study could be modified to include the thermal decomposition of NH_3 in the gas channel without catalyst for more accurate simulation.

In the literature, lots of research works on thermal catalytic decomposition of ammonia on various catalysts surface have been reported and thus relevant experimental data are used in this study. For example, the characteristics of NH_3 thermal decomposition on metals and compounds such as Fe, Ni, Pt, Ru, Ir, Pd, Ni–Pt, Ni/Ru, have been examined in details [28–31]. In the present study, it is considered that thermal decomposition can take place in the composite anode of SOFC with typical catalyst (Ni) loading [4]. Based on the experimental results, an analytical expression has been derived to describe the kinetics of thermal decomposition (mol m^{-3} s^{-1}) of NH_3 on the surface of Ni catalyst (typical Ni–YSZ cermet with a Ni loading of about 50 vol%) in SOFC [25]:

$$r = 4.0 \times 10^{15}\exp\left(-\frac{196200.0}{RT}\right)P_{NH_3} \tag{6}$$

where P_{NH_3} is the partial pressure of NH_3. It's considered that the reaction rate is mainly dependent on the partial pressure of NH_3 and the operating temperature.

The thermal catalytic decomposition of NH_3 (Eq. (1)) is endothermic and requires thermal energy input (J mol^{-1}). The thermal energy demand can be calculated from the enthalpy change of NH_3 thermal decomposition [32], which is tabulated in Table 2. In the temperature range of 600–1200 K, the

Table 2 – Thermal energy demand of NH_3 thermal decomposition [32].

Temperature (K)	Thermal energy demand (J mol^{-1})
600	51374
700	52618
800	53621
900	54411
1000	55013
1100	55451
1200	55746

thermal energy demand of NH_3 thermal decomposition can be approximately calculated as,

$$H_R = 40265.095 + 24.23214T - 0.00946T^2 \quad (7)$$

2.3. Computational fluid dynamics model

The fundamental transport phenomena in an SOFC are fluid flow, heat transfer and mass transfer. Due to small Reynolds number of the fluid flow, laminar flow conditions are usually applied. The heat/mass transfer phenomena in SOFCs are governed by the conservation laws for mass, momentum, energy, and species, which are summarized below [33]:

$$\frac{\partial(\rho U)}{\partial x} + \frac{\partial(\rho V)}{\partial y} = S_m \quad (8)$$

$$\frac{\partial(\rho UU)}{\partial x} + \frac{\partial(\rho VU)}{\partial y} = -\frac{\partial P}{\partial x} + \frac{\partial}{\partial x}\left(\mu\frac{\partial U}{\partial x}\right) + \frac{\partial}{\partial y}\left(\mu\frac{\partial U}{\partial y}\right) + S_x \quad (9)$$

$$\frac{\partial(\rho UV)}{\partial x} + \frac{\partial(\rho VV)}{\partial y} = -\frac{\partial P}{\partial y} + \frac{\partial}{\partial x}\left(\mu\frac{\partial V}{\partial x}\right) + \frac{\partial}{\partial y}\left(\mu\frac{\partial V}{\partial y}\right) + S_y \quad (10)$$

$$\frac{\partial(\rho c_p UT)}{\partial x} + \frac{\partial(\rho c_p VT)}{\partial y} = \frac{\partial}{\partial x}\left(k\frac{\partial T}{\partial x}\right) + \frac{\partial}{\partial y}\left(k\frac{\partial T}{\partial y}\right) + S_T \quad (11)$$

$$\frac{\partial(\rho UY_i)}{\partial x} + \frac{\partial(\rho VY_i)}{\partial y} = \frac{\partial}{\partial x}\left(\rho D_{i,m}^{eff}\frac{\partial Y_i}{\partial x}\right) + \frac{\partial}{\partial y}\left(\rho D_{i,m}^{eff}\frac{\partial Y_i}{\partial y}\right) + S_{sp} \quad (12)$$

where U and V are the velocity components in x and y directions; ρ is the gas density, which depends on local temperature and gas composition; μ is the viscosity of the gas mixture; k is the thermal conductivity; c_p is the heat capacity; $D_{i,m}^{eff}$ is the effective diffusion coefficient of species i in gas mixture and can be evaluated by Eq. (13)–(15); Y_i denotes the mass fraction of species i.

$$\frac{1}{D_{i,m}^{eff}} = \frac{\xi}{\varepsilon}\left(\frac{1}{D_{i,m}} + \frac{1}{D_{i,k}}\right) \quad (13)$$

$$D_{i,m} = \frac{1 - X_i}{\sum_{j\neq i}\frac{X_j}{D_{ij}}} \quad (14)$$

$$D_{i,k} = \frac{2r_p}{3}\sqrt{\frac{8RT}{\pi M_i}} \quad (15)$$

where X_i is the molar fraction of species i; M_i is the molecular weight of species i; D_{ij} is the binary diffusion coefficient of species i and j. The binary diffusion coefficients can be calculated as,

$$D_{ij} = \frac{0.0026T^{1.5}}{p\sqrt{M_{ij}}\sigma_{i,j}^2\Omega_D} \quad (16)$$

$$M_{ij} = \frac{2}{\frac{1}{M_i} + \frac{1}{M_j}} \quad (17)$$

where $\sigma_{i,j}$ is the mean characteristic length of species i and j; Ω_D is a dimensionless diffusion collision integral, which can be calculated as,

$$\sigma_{i,j} = \frac{\sigma_i + \sigma_j}{2} \quad (18)$$

$$\Omega_D = \frac{1.06036}{\tau^{0.1561}} + \frac{0.193}{\exp(0.47635\tau)} + \frac{1.03587}{\exp(1.52996\tau)} + \frac{1.76474}{3.89411\tau} \quad (19)$$

$$\tau = \frac{k_b T}{\varepsilon_{i,j}} \quad (20)$$

where $k_b = 1.3066 \times 10^{-23}$ (J K^{-1}) is the Boltzmann's constant. The values of σ_i and $\varepsilon_{i,j}$ can be found from reference [34].

In the porous electrodes, effective heat conductivity and heat capacity are used [35],

$$k = \varepsilon k_f + (1-\varepsilon)k_s \quad (21)$$

$$c_p = \varepsilon c_{p,f} + (1-\varepsilon)c_{p,s} \quad (22)$$

where ε is the porosity of the electrode; k_f and k_s are the heat conductivity (W m^{-1} K^{-1}) of the fluid and solid, respectively; $c_{p,f}$ and $c_{p,s}$ are the heat capacity (J kg^{-1} K^{-1}) of the fluid and solid, respectively.

The source term S in continuity equation (Eq. (8)) represents the mass change due to electrochemical reaction at the electrode–electrolyte interface. Thus the source term is non-zero at the electrode–electrolyte interface and zero in other regions. At the anode–electrolyte interface, the source term for continuity equation can be written as,

$$S_m = \frac{JM_{H_2O}}{2F\Delta y} - \frac{JM_{H_2}}{2F\Delta y} \quad (23)$$

where Δy is the width of the control volume in y direction at the anode–electrolyte interface. At the cathode–electrolyte interface, this source term is calculated as,

$$S_m = -\frac{JM_{O_2}}{4F\Delta y} \quad (24)$$

The Darcy's law is used as source terms in momentum equations (Eqs. 9 and 10) so that the momentum equations are valid for both the gas channels and the porous electrodes [35];

$$S_x = \frac{\mu U}{B_g} \quad (25)$$

$$S_y = \frac{\mu V}{B_g} \quad (26)$$

where B_g is the permeability of the porous electrodes (m^2).

The source term (W m^{-3}) in energy equation (Eq. (11)) includes: (1) heat generation due to electrochemical entropy

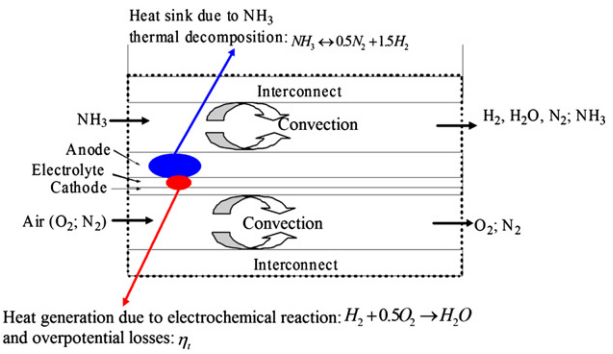

Fig. 2 – Heat sink and heat generation in NH_3-fueled SOFC.

change and irreversible overpotentials [33] and (2) heat energy demand for thermal decomposition of NH_3 (Eq. (1) and (5)). The overall heat sink and heat generation in the SOFC is schematically shown in Fig. 2. In the porous anode, thermal decomposition of NH_3 takes place and thus the source term can be written as,

$$S_T = -rH_R \tag{27}$$

In the dense electrolyte, the source term includes the irreversible loss through entropy change and activation losses via electrochemical reaction (at the electrode–electrolyte interface), as well as ohmic overpotential of the electrolyte. These losses are assumed to evenly distributed in the electrolyte and thus the source term can be written as,

$$S_T = -\frac{JT\Delta S}{2Fd_e} + \frac{J\eta_t}{d_e} \tag{28}$$

where ΔS is the entropy change of the electrochemical reaction (J K^{-1} mol^{-1}) and can be found from reference [32]; d_e is the thickness of electrolyte; η_t (V) is the total overpotential loss, which can be calculated as,

$$\eta_t = V - E \tag{29}$$

It should be mentioned that the ohmic losses at the electrodes are not included in calculating the total overpotential loss, as they are usually small, compared with the electrolyte ohmic loss and the activation losses [36]. However, the ohmic loss of the electrodes can be easily included in the electrochemical model if the conductivity of SOFC electrodes is low.

The source terms in species equations (Eq. (12)) can be calculated in the way similar to the source term for continuity equation (Eq. (8)). However, in the anode, the thermal decomposition of NH_3 should be included.

In this study, the electrochemically consumed H_2 fuel comes from NH_3 thermal decomposition (Eq. (1)). Thus, electrochemical consumption of N mol H_2 fuel is equivalent to consumption of N/1.5 mol NH_3 fuel. With a gas channel width of w (in a direction perpendicular to the x–y plane in Fig. 1), the amount (N, mol s^{-1}) of electrochemically consumed H_2 fuel can be evaluated as,

$$N = \frac{\bar{J}Lw}{2F} \tag{30}$$

where L is the length of the SOFC cell, $\bar{J}$ is the average current density (A m^{-2}).

The inlet gas velocity (U_{in}, m s^{-1}) of NH_3 can be converted to molar flow rate (F_{in}, mol s^{-1}) as,

$$F_{in} = \frac{U_{in}H_F w\rho}{M_{NH_3}} \tag{31}$$

where H_F is the height of gas channel (1 mm in the present study), ρ is the density of NH_3 (kg m^{-3}) and M_{NH_3} is the molecular weight of NH_3 (kg mol^{-1}). Obviously $H_F w$ is the cross-sectional area (m^2) of the gas channel. The fuel utilization factor (η_F) [37], can thus be evaluated as,

$$\eta_F = \frac{N}{1.5F_{in}} = \frac{\bar{J}LM_{NH_3}}{3FU_{in}H_F\rho} \tag{32}$$

3. Numerical methodology

3.1. Boundary conditions

The boundary conditions for the present model are briefly summarized here. At the inlet ($x = 0$), a constant flow velocity is specified for the gas flow channels, while zero gas velocity is specified for the solid part. Similarly, constant gas compositions are specified at the inlets of the gas flow channels and constant temperature is specified at the inlet for both the gas flow channels and the solid part. At the bottom and the top of the computation zone ($y = 0$ and $y = y_M$ in Fig. 1), thermally adiabatic conditions are assumed (zero temperature gradient). At the outlet of the computation domain ($x = x_L$), zero temperature gradient, zero velocity gradient, and zero mass fraction gradient are assumed for gas flow channels, while zero velocity is assumed for the solid part.

3.2. Numerical scheme

The governing equations are discretized and solved using the finite volume method [38]. The boundary conditions and the

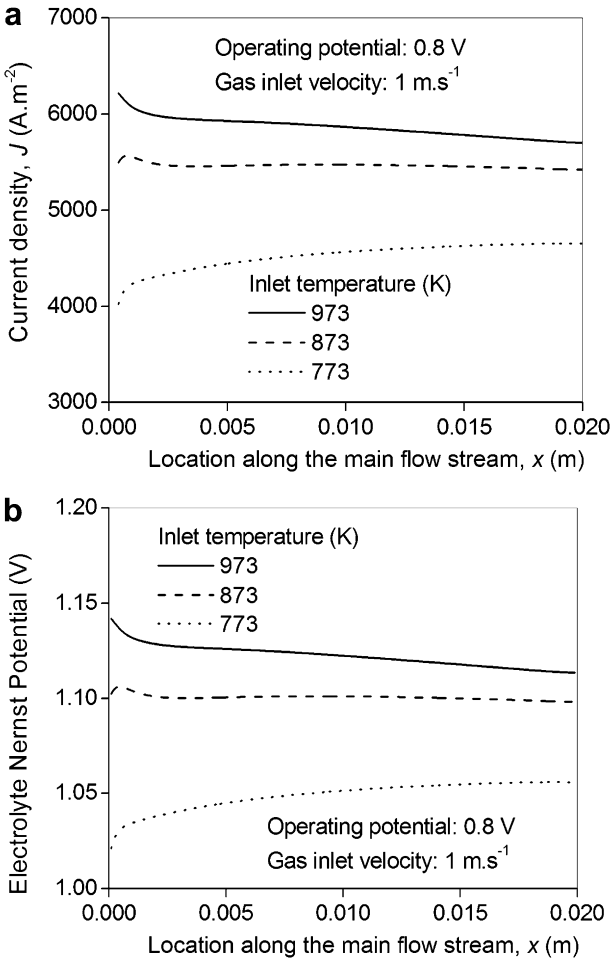

Fig. 3 – Effect of temperature on NH_3-fueled SOFC performance – (a) Distribution of current density; (b) Distribution of electrolyte Nernst potential.

detailed calculation procedures can be found in the previous publication and thus not repeated here [39]. It should be mentioned that the electrochemical model and the chemical model are linked with the CFD model through source terms. In the iteration, the current density and chemical reaction rate are obtained from the electrochemical model and the chemical model for calculating the source terms in CFD model. Then the CFD model is solved to update the temperature, gas composition, fluid velocity in SOFC. With the updated gas composition and temperature, the electrochemical model and chemical model are solved again to update the current density and chemical reaction rate. Computation is repeated until convergence is obtained. The in-house CFD code is written in FORTRAN.

4. Results and discussion

Before performing parametric simulations, the model should be validated by using experimental data. In the literature, there are many available experimental data for model validation and parameter determination. The electrochemical model, chemical model and CFD model have been validated by using the literature data and presented in the previous publications [25,38]. Numerical experiments have been carried out to ensure grid independence of the results. The dimensions and typical structural/operating parameters for NH_3-fueled SOFC are summarized in Table 1. It should be mentioned that the length of SOFC in literature varies considerably. In the present study, the cell length of 20 mm from the literature [23,40] is used in the simulation, as a larger cell length requires considerably more computation resources.

4.1. *Temperature effect*

The effect of inlet temperature on performance of NH_3-fueled SOFC is shown in Fig. 3. It is found that both the current density and electrolyte Nernst potential increase with increasing inlet temperature, indicating that higher electric output can be obtained at higher inlet temperature. More importantly, the distributions of local current density and electrolyte Nernst potential are quite different at different temperatures. At a higher inlet temperature (i.e. 973 K), the local current density and electrolyte Nernst potential monotonically decrease along the main flow stream, which is similar to a H_2-fueled SOFC [39]. For comparison, at a lower inlet temperature (i.e. 773 K), both the local current density and electrolyte Nernst potential increase significantly near the inlet, followed by gradual increase along the main flow stream in the downstream. The difference is mainly caused by different distributions of H_2 molar fraction at different temperatures. In the present study, the molar fraction of H_2 at the SOFC inlet is zero, since NH_3 is used as a fuel for SOFC. For both high and low temperatures, the molar fraction of H_2 increases along the flow channel due to thermal decomposition of NH_3 in the SOFC anode (Fig. 4). At an inlet temperature of 973 K, the molar fraction of H_2 increases rapidly near the inlet from 0.0 to be higher than 0.5 in the porous anode, followed by a slight increase in the downstream (Fig. 4a). Due to the high molar fraction of H_2 near the inlet (so that the ratio of $P^I_{H_2}(P^I_{O_2})^{0.5}/P^I_{H_2O}$ decreases along the channel), it is similar to an SOFC directly running on H_2 and it is the reason

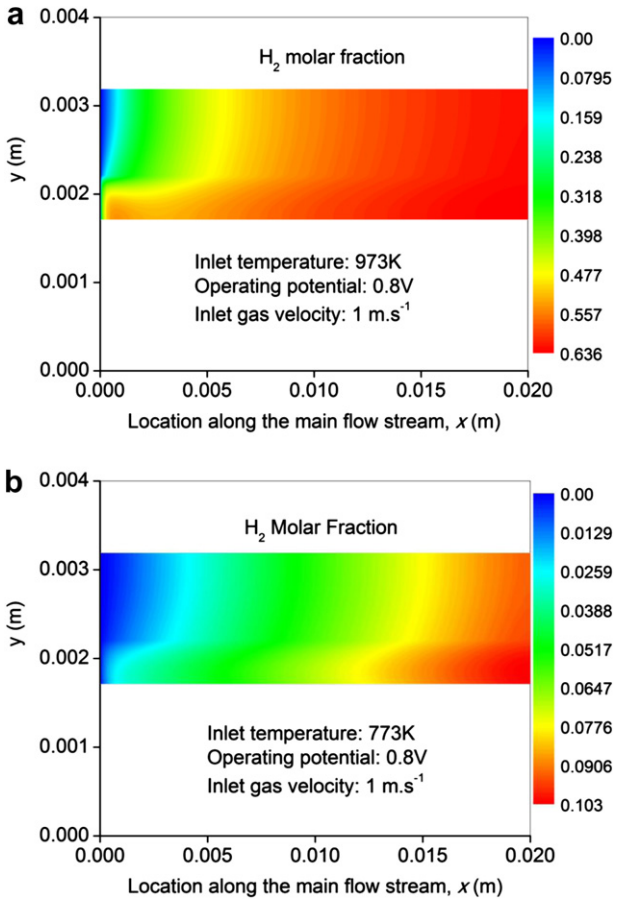

Fig. 4 – Distribution of H_2 molar fraction in NH_3-fueled SOFC – (a) Inlet temperature: 973 K; (b) Inlet temperature: 773 K; Note: in y-axis, from 0 to 0.5 mm and from 3.2 mm to 3.7 mm are interconnectors; from 0.5 mm to 1.5 mm is the cathode (air) channel; from 1.5 mm to 1.6 mm is the porous cathode; from 1.6 mm to 1.7 mm is the dense electrolyte; from 1.7 mm to 2.2 mm is the porous anode; from 2.2 mm to 3.2 mm is the anode (fuel) channel.

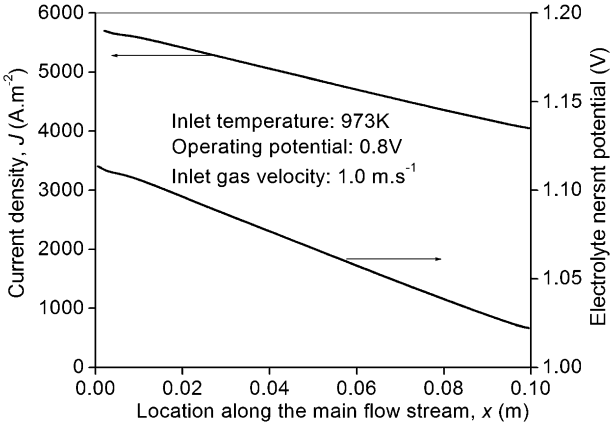

Fig. 5 – Distribution of current density and electrolyte Nernst potential in NH_3-fueled SOFC with cell length of 10 cm.

why the current density and electrolyte Nernst potential are similar to those of the H_2-fueled SOFC [39]. For comparison, at an inlet temperature of 773 K, the molar fraction of H_2 increases steadily from 0.0 at the inlet to be slightly higher than 0.1 at the outlet of SOFC (Fig. 4b). From Eq. (4) it can be seen that the electrolyte Nernst potential is related to the ratio of $P^I_{H_2}/P^I_{H_2O}$, which means the electrolyte Nernst potential is more sensitive to H_2 molar fraction at a lower molar fraction of H_2. For example, an increase of H_2 molar fraction from 0.001 to 0.01 can increase the ratio of $P^I_{H_2}/P^I_{H_2O}$ by 10 times. The relatively large variation of $P^I_{H_2}/P^I_{H_2O}$ explains why there is a considerable increase in both local current density and electrolyte Nernst potential near the inlet at a temperature of 773 K (Fig. 3). The average power densities are calculated to be 4688.3 W m^{-2} and 3620.5 W m^{-2} at 973 K and 773 K, respectively. The fuel utilization factor at 973 K and 773 K are about 3.7% and 3.0%, respectively. The very low fuel utilization factor is mainly caused by small cell length (2 cm) used in the present study. An increase in cell length from 2 cm to 10 cm can increase the fuel utilization factor to be about 15.3%. The fuel utilization factor does not linearly increase with increasing cell length is because the average current density decreases with increasing cell length, as can be seen from the distributions of current density and Nernst potential in Fig. 5. However, as the computation time is significantly increased with increasing cell length (without increasing the grid size), the following simulations are performed for a cell length of 2 cm, which is also in line with some studies in literature [23,40].

Since H_2 is produced from NH_3 thermal decomposition, the kinetics of NH_3 thermal decomposition at different temperatures are investigated and shown in Fig. 6. At a high inlet temperature (973 K), the rate of NH_3 thermal decomposition is very high (>6×10^4 mol m^{-3} s^{-1}) near the inlet in the porous anode and decreases rapidly in the downstream (Fig. 6a). Using a logarithmic scale, it can be seen that the rate of NH_3 thermal decomposition is about 10^3 mol m^{-3} s^{-1} at the middle of SOFC and decreases to be on the order of 10^2 mol m^{-3} s^{-1} in the downstream of the SOFC (Fig. 6b). For comparison, the rate of NH_3 thermal decomposition does not vary too much at an

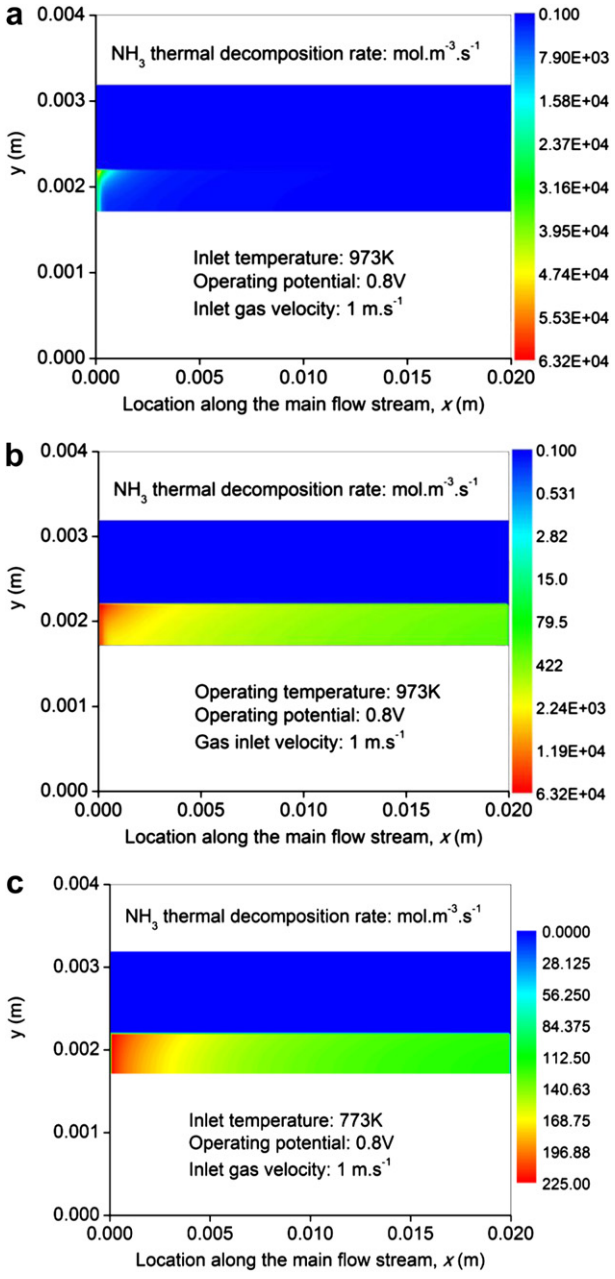

Fig. 6 – NH_3 thermal decomposition in SOFC – (a) Inlet temperature: 973 K; (b) Inlet temperature: 973 K, logarithmic scale; (c) Inlet temperature: 773 K.

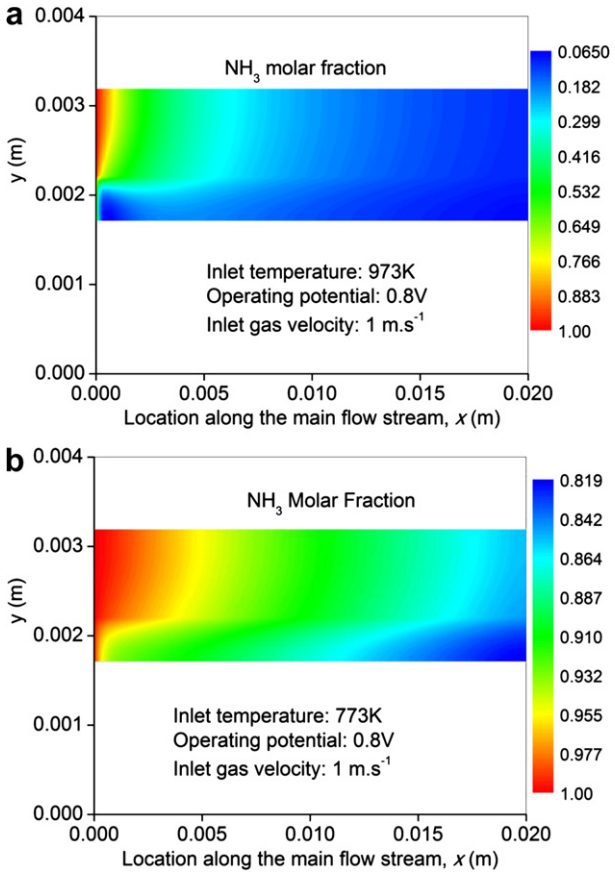

Fig. 7 – Distribution of NH_3 molar fraction in NH_3-fueled SOFC – (a) Inlet temperature: 973 K; (b) Inlet temperature: 773 K.

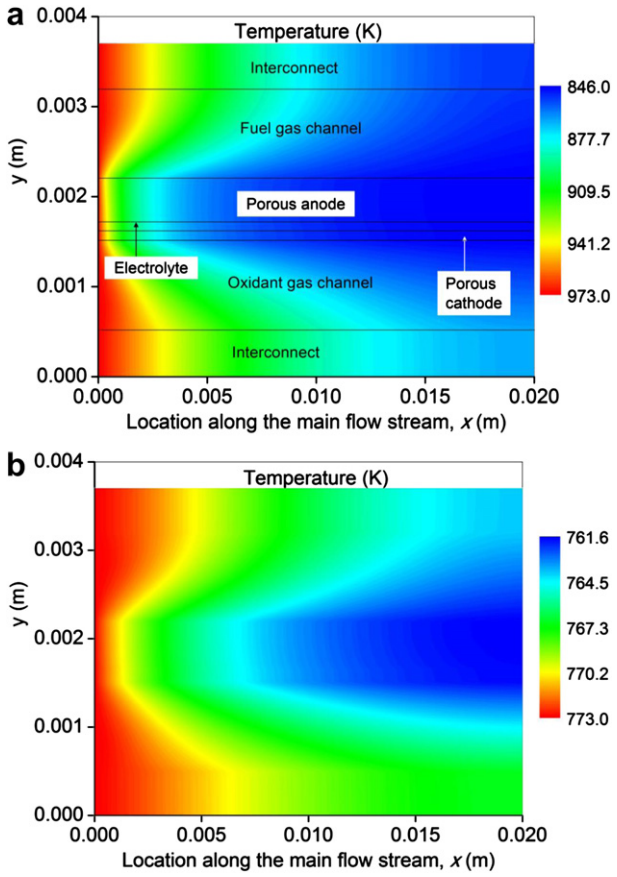

Fig. 8 – Temperature of NH_3-fueled SOFC – (a) Inlet temperature: 973 K; (b) Inlet temperature: 773 K.

inlet temperature of 773 K – decreases from about 225 mol m^{-3} s^{-1} at the inlet to about 112 mol m^{-3} s^{-1} at the outlet of SOFC (Fig. 6c). As a result, the molar fraction of NH_3 decreases from 1.0 at the inlet to be about 0.06 near the inlet (in the porous anode), due to very high rate of NH_3 thermal decomposition at an inlet temperature of 973 K (Fig. 7a). It should be mentioned that in the immediate downstream of the locally low NH_3 molar fraction, there is a slight increase in NH_3 molar fraction in the porous anode, due to diffusion and permeation of NH_3 from the gas channel to the porous electrode. At an inlet temperature of 773 K, the molar fraction of NH_3 decreases gradually from 1.0 at the inlet to be about 0.85 at the outlet (Fig. 7b).

The temperature field of SOFC is determined by the source term in energy equation (Eq(2). 27, 28). For NH_3-fueled SOFC, this source term depends on 3 factors: (1) NH_3 thermal decomposition for H_2 and N_2 generation; (2) entropy change of the electrochemical reaction; and (3) irreversible overpotential loss, including the ohmic, activation, and concentration overpotentials. The first factor is highly endothermic while both (2) and (3) are exothermic. The considerable temperature decrease along the NH_3-fueled SOFC indicates that the thermal energy demand for NH_3 thermal decomposition is higher than the heat generation by the electrochemical reaction and the overpotential losses (Fig. 8). The result is consistent with experimental observation, which showed considerable temperature decrease in NH_3-fueled SOFC [41]. More importantly, it is found that the temperature gradient in SOFC is very high at a high temperature. At an inlet temperature of 973 K, the SOFC temperature decreases by more than 100 K in only 5 mm downstream of the inlet and the temperature difference between the inlet and outlet is about 130 K (Fig. 8a). This is because the endothermic thermal decomposition of NH_3 is highly temperature dependent. At a high

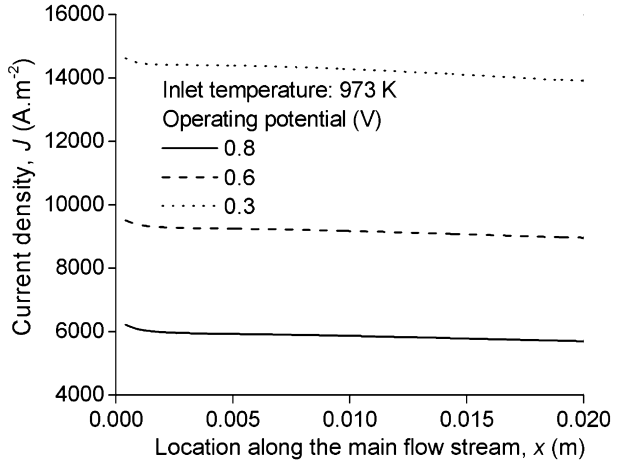

Fig. 9 – Effect of operating potential on NH_3-fueled SOFC performance.

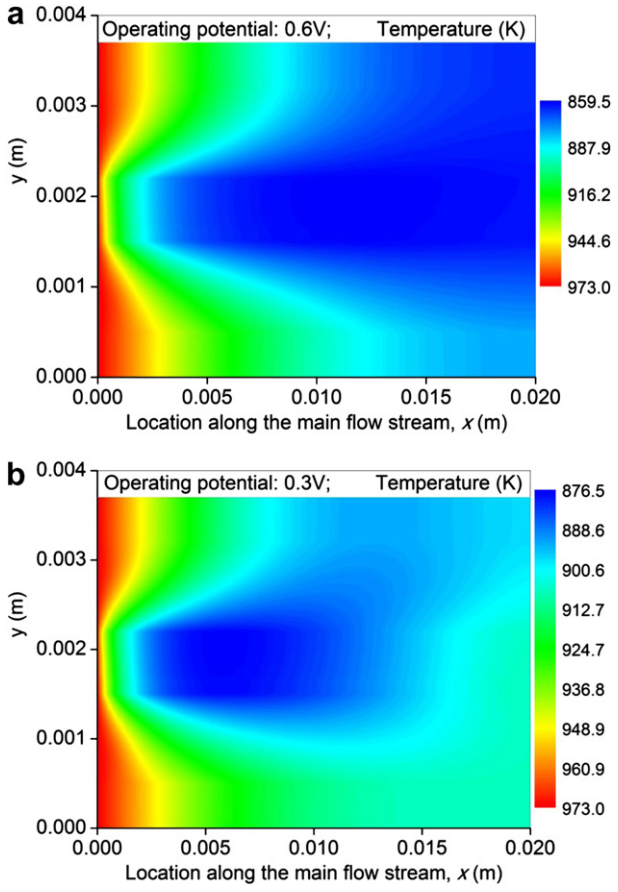

Fig. 10 – Temperature of NH_3-fueled SOFC – (a) Operating potential: 0.6 V; (b) Operating potential: 0.3 V.

temperature (i.e. 973 K), the rate of NH_3 thermal decomposition is high, consuming a considerable amount of heat, which in turn decrease the SOFC temperature considerably (Fig. 8). The high temperature reduction also explains why the rate of NH_3 thermal decomposition decreases rapidly along the SOFC (Fig. 6), which in turn decreases the heat demand in the downstream.

From the above analysis, it can be seen that the inclusion of NH_3 thermal decomposition in SOFC complicates the transport and reaction processes and significantly influences both the temperature field and the electrochemical performance of SOFC. One can increase the electric output of the SOFC by increasing the temperature, but the very large temperature gradient in the SOFC at high inlet temperature must be considered carefully in stack design.

4.2. *Strategies to reduce the temperature difference in SOFC*

As already mentioned in the previous section, the temperature field of NH_3-fueled SOFC depends on 3 factors. We may reduce the temperature gradient by adjusting these 3 factors. Since the exothermic electrochemical reaction and the overpotential losses depends on the current density, it is possible to increase the heat generation by operating the SOFC at higher current density, or in other words, at lower operating potential. As expected, the current density is increased considerably when the operating potential is decreased from 0.8 V to 0.3 V (Fig. 9). As the operating potential is reduced from 0.8 V to 0.6 V, the temperature difference between the inlet and outlet is reduced from about 130 K to about 115 K (Fig. 10a). With a further reduction in operating potential (to 0.3 V), the inlet/outlet temperature difference is further reduced and the temperature in the downstream of SOFC starts to increase along the gas channel (Fig. 10b). However, it should be also mentioned that the temperature gradient in the upstream is still high due to high rate of NH_3 decomposition. As heat generation increases with decreasing operating potential, the cell temperature starts to increase in the downstream of the cell, generating a "cold spot" in the upstream (Fig. 10b). The average current density is increased from 5860.4 A m^{-2} at 0.8 V to 9160.1 A m^{-2} at 0.6 V, and further to 14232.4 A m^{-2} at 0.3 V. As a result, the fuel utilization factor is increased from 3.7% at 0.8 V to about 5.8% at 0.6 V, and 8.9% at 0.3 V. The average power density is increased from 4688.3 W m^{-2} at 08 V to 5496.1 W m^{-2} at 0.6 V, but with a further decrease in operating potential to 0.3 V, the average power density is decreased considerably to 4269.7 W m^{-2}. The variation of power density with operating potential is in line with other electrochemical modeling studies on SOFC, which show maximum power

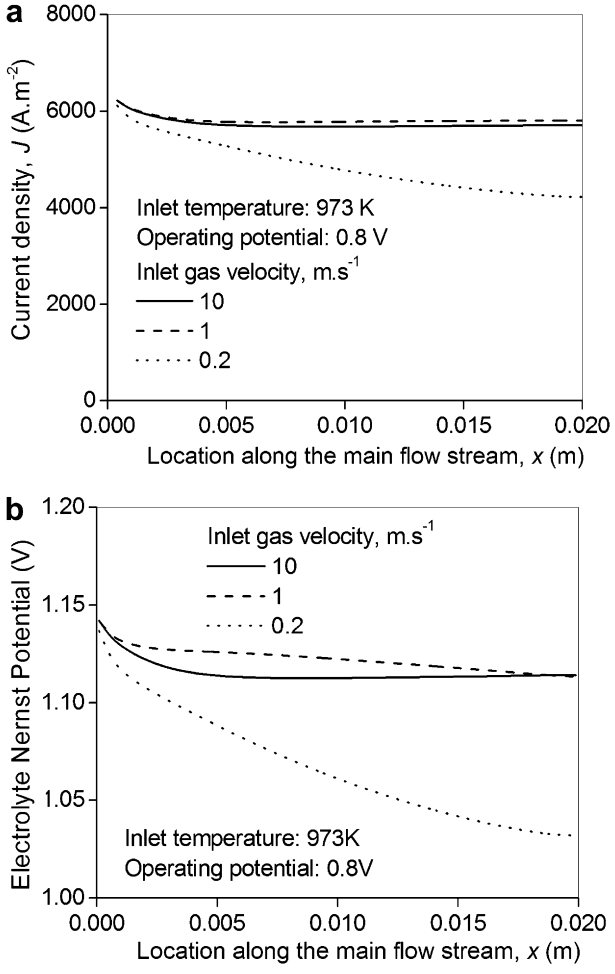

Fig. 11 – Effect of inlet gas velocity on NH_3-fueled SOFC performance – (a) Distribution of current density; (b) Distribution of electrolyte Nernst potential.

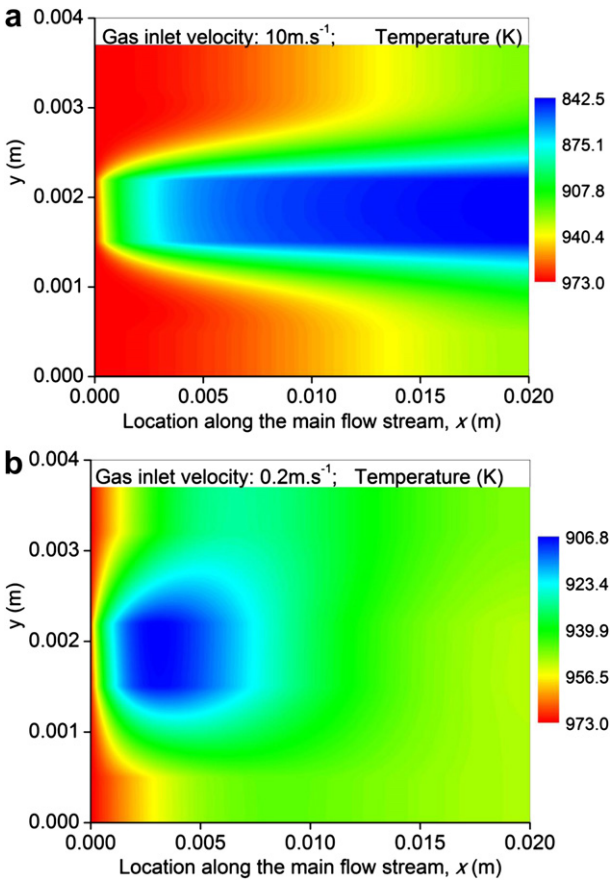

Fig. 12 – Temperature of NH_3-fueled SOFC – (a) Inlet gas velocity: 10 m s^{-1}; (b) Inlet gas velocity: 0.2 m s^{-1}.

density at optimal operating potential. Therefore, reducing the operating potential can reduce the inlet/outlet temperature difference, increase fuel utilization factor but too low potential may result in a low electric output. In addition, the high temperature gradient ("cold spot") in the upstream (near the inlet) remains to be further reduced.

The effects of inlet gas velocity on the SOFC performance and temperature field are investigated and discussed in the subsequent paragraphs. It is found that increasing the inlet gas velocity from 1.0 m s^{-1} to 10.0 m s^{-1} decreases slightly both the current density and the Nernst potential (Fig. 11). As a result, the average current density is slightly decreased from 5860.4 A m^{-2}–5737 A m^{-2}, as the inlet gas velocity is increased from 1.0 to 10.0 m s^{-1}, leading to a small decrease in average power density from 4688.3 W m^{-2} to 4589.6 W m^{-2}. Moreover, the fuel utilization factor is considerably decreased to be only 0.36% at an inlet gas velocity of 10.0 m s^{-1}. This is different from H_2-fueled SOFC, in which the current density, electrolyte

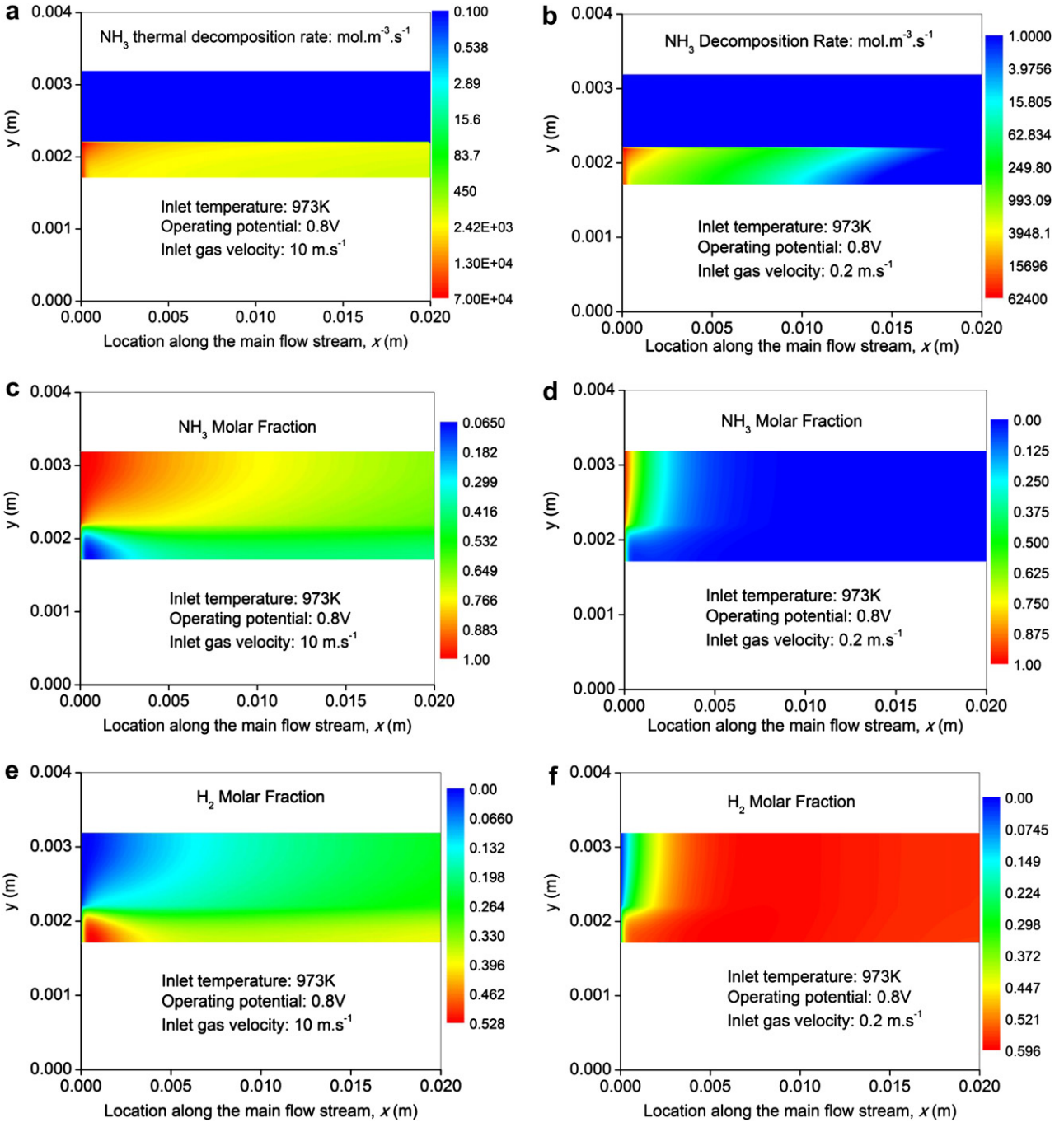

Fig. 13 – Effect of inlet gas velocity – (a) NH_3 decomposition rate at 10 m s^{-1}; (b) NH_3 decomposition rate at 0.2 m s^{-1}; (c) NH_3 molar fraction at 10 m s^{-1}; (d) NH_3 molar fraction at 0.2 m s^{-1}; (e) H_2 molar fraction at 10 m s^{-1}; (f) H_2 molar fraction at 0.2 m s^{-1} (g) H_2O molar fraction at 10 m s^{-1}; (h) H_2O molar fraction at 0.2 m s^{-1} (i) O_2 molar fraction at 10 m s^{-1}; (j) O_2 molar fraction at 0.2 m s^{-1}.

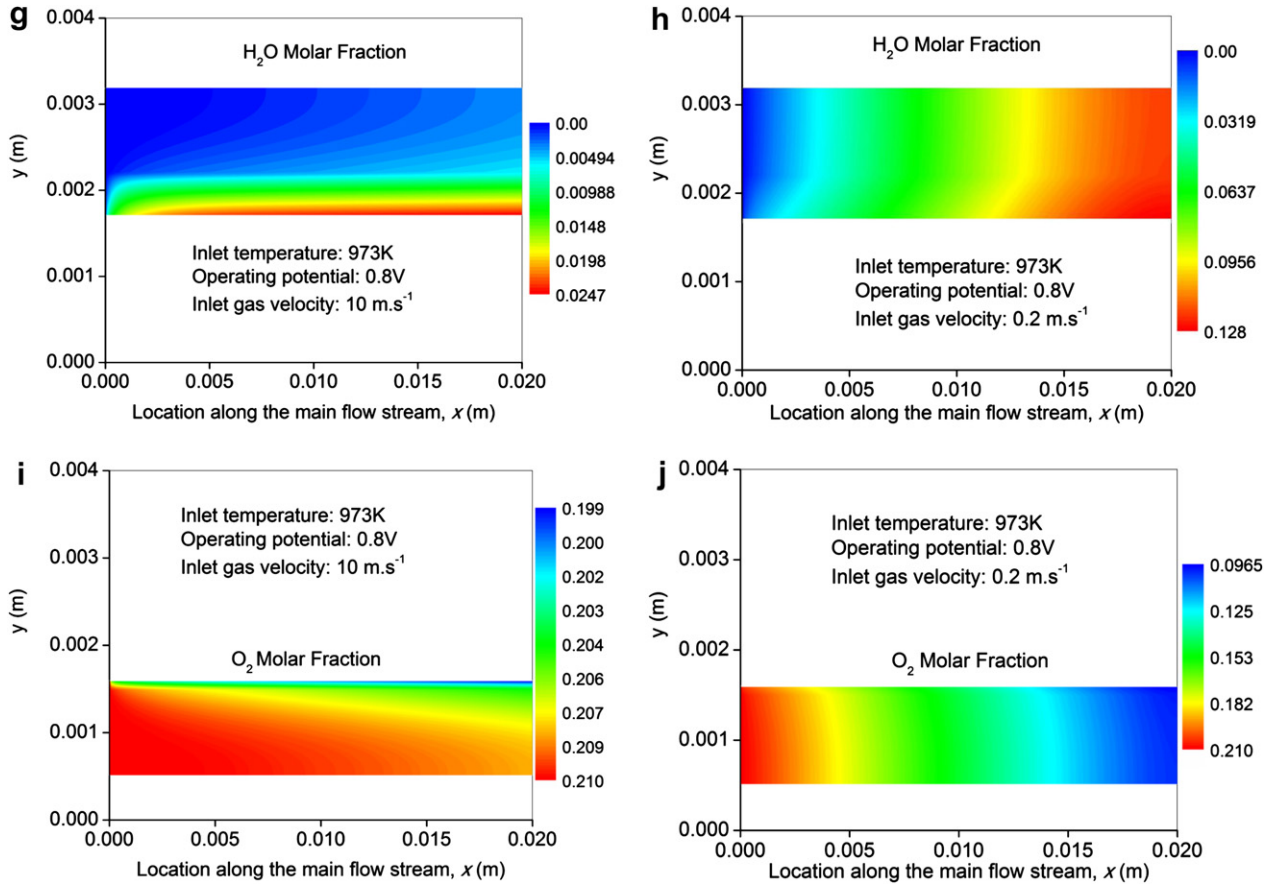

Fig. 13 – *(continued)*

Nernst potential, and average power density increase with increasing gas velocity [38]. In addition, a decrease in inlet gas velocity to 0.2 m s^{-1} decreases significantly both the current density and electrolyte Nernst potential. And the average current density and power density are decreased to 4850.8 A m^{-2} and 3880.6 W m^{-2}, respectively. However, the fuel utilization factor is significantly improved to be about 15.2% at an inlet gas velocity of 0.2 m s^{-1}. The dependence of current density and electrolyte Nernst potential on gas velocity is mainly due to the variation in gas composition and will be discussed later. It should be noted that the reduction in current density will reduce the heat generation from electrochemical reaction and overpotential losses. Therefore, the inlet/outlet temperature difference is slightly increased as the inlet gas velocity is increased from 1 m s^{-1} to 10 m s^{-1}, despite of higher heat transfer between the gas and the solid structure (Fig. 12a). For comparison, the inlet/outlet temperature difference of SOFC is considerably decreased at a gas inlet velocity of 0.2 m s^{-1} (Fig. 12b). The "cold spot" in the upstream is a result of temperature reduction by NH_3 decomposition in the upstream and temperature increase by electrochemical reaction and overpotential loss in the downstream. The difference in temperature field at various gas velocities results from the different current density and different rates of NH_3 thermal decomposition. As can be seen from Fig. 13a, the NH_3 thermal decomposition rate is slightly higher at a gas velocity of 10 m s^{-1} than at a gas velocity of 1.0 m s^{-1}, resulting in higher heat demand. For comparison, the rate of NH_3 thermal decomposition is decreased to be very small (about 1.0 mol m^{-3} s^{-1}) in the downstream of the SOFC at an inlet gas velocity of 0.2 m s^{-1} (Fig. 13b), leading to smaller or even zero heat consumption. At a high gas velocity (10 m s^{-1}), more NH_3 can be transported from the gas channel to the porous electrode through permeation. In addition, as more NH_3 is supplied to the anode at a high inlet gas velocity, the molar fraction of NH_3 only decreases from 1.0 at the SOFC inlet to about 0.6 at the outlet (Fig. 13c). The higher NH_3 molar fraction can lead to higher rate of NH_3 thermal decomposition at higher inlet gas velocity, since the decomposition rate is proportional to the partial pressure of NH_3 (Eq. (6)). For comparison, the molar fraction of NH_3 decreases from 1.0 to 0.0 in the downstream of SOFC at an inlet gas velocity of 0.2 m s^{-1}, as much less NH_3 is supplied to the anode channel (Fig. 13d). And this can decrease the rate of NH_3 thermal decomposition at a lower inlet gas velocity (Fig. 13b).

In order to understand the effect of inlet gas velocity on current density and electrolyte Nernst potential, the distributions of gas composition in SOFC are investigated. At a higher inlet gas velocity (10 m s^{-1}), the H_2 molar fraction increases from 0.0 at the inlet to be about 0.3 at the outlet (Fig. 13e), which is lower than at an inlet gas velocity of 1.0 m s^{-1} (Fig. 4a). This is because the supply of larger amount of NH_3 dilutes the concentration of H_2, despite of higher rate of NH_3 thermal decomposition. For comparison, at an inlet gas

velocity of 0.2 m s^{-1}, the molar fraction of H_2 increases quickly to be about 0.6 near the inlet, followed by small variation in the downstream as NH_3 is completely decomposed (Fig. 13f). From the Nernst equation, it is expected that the lower molar fraction of H_2 at a high inlet gas velocity tends to decrease the electrolyte Nernst potential. However, the actual current density and electrolyte Nernst potential only slightly decreases when the inlet gas velocity is increased from 1.0 m s^{-1} to 10.0 m s^{-1} (Fig. 11). The reason is that at a higher gas velocity (10 m s^{-1}), the molar fraction of H_2O in the anode is decreased while the molar fraction of O_2 is increased (Fig. 13g and i), which tends to increase the electrolyte Nernst potential and the current density. The combined effects result in a slight decrease of electrolyte Nernst potential and current density with increasing gas velocity (Fig. 11). At a low inlet gas velocity (0.2 m s^{-1}), the molar fraction of H_2O increases considerably (Fig. 13h) while the molar fraction of O_2 decreases more significantly than at a higher gas velocity (Fig. 13j), which considerably decreases both the electrolyte Nernst potential and thus the current density (Fig. 11).

From the above analysis, it can be seen that the temperature gradient of SOFC can be reduced by operating the SOFC at a lower potential, thus producing a higher current density and more heat generation to compensate heat sink due to NH_3 thermal decomposition. It can also improve the fuel utilization factor. However, there is an optimal operating potential to achieve the highest average power density. A high inlet gas velocity is beneficial to improve the electric output of H_2-fueled SOFC, but degrades the electric output of NH_3-fueled SOFC. In addition, the fuel utilization factor is significantly decreased at a high inlet gas velocity. At a low inlet gas velocity (0.2 m s^{-1}), the temperature gradient can be reduced and the fuel utilization factor can be increased. However, the electric output (average current density and power density) is decreased at an inlet gas velocity of 0.2 m s^{-1}. In practice, constant fuel utilization factor can be maintained by adjusting the operating parameters. For example, an increase in inlet temperature (i.e. from 873 K to 973 K) can decrease the inlet gas density at a given inlet gas velocity, leading to a lower F_{in} (Eq. (32)). In order to maintain a constant fuel utilization factor, the average current density should be reduced accordingly, decreases the amount of heat generation. Since NH_3 catalytic thermal decomposition (endothermic) largely determines the temperature field of NH_3-fueled SOFC, the temperature gradient could be further higher in order to maintain a constant fuel utilization factor at a high inlet temperature. As discussed in the previous section, higher current density (higher fuel utilization factor) is useful to reduce the temperature gradient at a higher temperature. This is different from H_2-fueled SOFC. For a H_2-fueled SOFC, an increase in inlet temperature decreases the gas density thus requires lower current density in order to maintain a constant fuel utilization factor, which in turn decreases the temperature gradient in SOFC stack. Therefore, all the factors should be carefully considered in determining the optimal operating conditions of NH_3-fueled SOFC. If the SOFC is specified mainly to produce high power density, the SOFC should be operated at an optimal potential. If a high fuel utilization factor is desired, then a large cell length, a low operating potential and a low inlet gas velocity should be chosen.

5. Conclusion

A 2D thermo-electrochemical model is developed to study the performance of a NH_3-fueled SOFC, by integrating a 2D CFD model with an electrochemical model and a chemical model. The conjugate heat transfer, mass transfer, as well as chemical/electrochemical reactions in SOFC are fully considered.

It if found that the inclusion of NH_3 thermal decomposition in SOFC significantly impacts the SOFC electric output and the temperature field. In addition, the inlet temperature considerably influences the SOFC performance. At a higher inlet temperature (973 K), both current density and electrolyte Nernst potential decrease monotonically along the SOFC channel. While at a lower inlet temperature (773 K), the current density and electrolyte Nernst potential increase rapidly near the inlet, followed by gradual increase in the downstream. At an inlet temperature of 973 K, the rate of NH_3 thermal decomposition is very high (higher than 60000 mol m^{-3} s^{-1}) near the inlet but decreases rapidly in the downstream, due to a significant decrease in SOFC temperature. For comparison, the rate of NH_3 thermal decomposition is in the order of 100 mol m^{-3} s^{-1} and does not vary much along the SOFC channel at an inlet temperature of 773 K. Although higher inlet temperature is desirable to achieve higher electric output of the SOFC, the large temperature gradient in the SOFC at a higher temperature must be considered carefully.

Simulations are conducted to evaluate possible ways to reduce the temperature gradient in SOFC at elevated temperature. It is found that decreasing the operating potential can increase the fuel utilization factor considerably. It can also reduce the temperature gradient in the SOFC, particularly in the downstream. However, the "cold spot" in the upstream remains to be solved. And the highest average power density occurs at an optimal operating potential. Increasing the inlet gas velocity from 1.0 m s^{-1} to 10.0 m s^{-1} significantly decreases the fuel utilization factor but slightly decreases the electric output of NH_3-fueled SOFC, which is different from H_2-fueled SOFC. In addition, as the rate of NH_3 thermal decomposition and current density only vary slightly with increasing inlet gas velocity, the temperature field does not change much when the inlet gas velocity is increased from 1.0 m s^{-1} to 10.0 m s^{-1}. For comparison, reducing the inlet gas velocity from 1.0 m s^{-1} to 0.2 m s^{-1} is more effective in reducing the temperature gradient of SOFC, mainly due to the considerable reduction in NH_3 thermal decomposition rate. The fuel utilization factor is also significantly improved at an inlet gas velocity of 0.2 m s^{-1}. However, the electric output of SOFC is considerably decreased at a low inlet gas velocity. All these factors should be carefully considered in the design of optimal operating conditions.

Acknowledgments

The author is indebted to the anonymous referees for their critical reviews and constructive comments/suggestions on the original manuscript. The financial support from The Hong Kong Polytechnic University for newly recruited Assistant Professors (Project No. 1-ZV6M) is acknowledged.

Nomenclature

B_g	Electrode permeability, m^2
c_p	Heat capactity, J kg^{-1} K^{-1}
d_a	Thickness of anode, μm
d_c	Thickness of cathode, μm
d_e	Thickness of electrolyte, μm
$D_{i,m}^{eff}$	Effective diffusion coefficient of species i in gas mixture, cm^2 s^{-1}
$D_{i,k}$	Knudsen diffusion coefficient of i, cm^2 s^{-1}
$D_{i,j}$	Binary diffusion coefficient of i and j, cm^2 s^{-1}
E	Equilibrium potential, V
E_0	Reversible potential at standard condition, V
F	Faraday constant, 9.6485×10^4 C mol^{-1}
F_{in}	Molar flow rate of NH_3 at the SOFC inlet , mol s^{-1}
H_F	Height of gas flow channel, m
H_R	Heat demand for NH_3 thermal decomposition, J mol^{-1}
J	Current density, $A.m^{-2}$
k	Thermal conductivity, W m^{-1} K^{-1}
L	Length of the SOFC cell, m
M_i	Molecular weight of species i, kg mol^{-1}
N	Electrochemical consumption rate of H_2 fuel, mol s^{-1}
P	Operating pressure, bar
P_i^I	Partial pressure of species i at electrode–electrolyte interface, bar
r	Reaction rate of NH_3 thermal decomposition, mol m^{-3} s^{-1}
r_p	Mean pore radius of electrode, μm
R	Universal gas constant, 8.3145 J mol^{-1} K^{-1}
S_m	Source term in continuity equation, kg m^{-3} s^{-1}
S_x,S_y	Source terms in momentum equations, kg m^{-2} s^{-2}
S_T	Source terms in energy equations, W m^{-3}
S_{sp}	Source terms in species equations, kg m^{-3} s^{-1}
T	Inlet temperature, K
U	Velocity in x direction, m s^{-1}
U_{in}	Gas velocity at the SOFC inlet, m s^{-1}
V	SOFC operating potential, V; Velocity in y direction, m s^{-1}
X	Molar fraction of species i
Y	Mass fraction of species i
ε	Electrode porosity
ξ	Electrode tortuosity
$\sigma_{i,j}$	Mean characteristic length of species i and j
Ω_D	Dimensionless diffusion collision integral
ρ	Density of the gas mixture, kg m^{-3}
μ	Viscosity of gas mixture, kg m^{-1} s^{-1}
$\eta_{act,a}$	Activation overpotential at anode, V
$\eta_{act,c}$	Activation overpotential at cathode, V
η_F	Fuel utilization factor
η_{ohmic}	Ohmic overpotential of the electrolyte, V

REFERENCES

[1] Hawkes AD, Aguiar P, Hernandez-Aramburo CA, Leach MA, Brandon NP, Green TC, et al. Techno-economic modeling of a solid oxide fuel cell stack for micro combined heat and power. J Power Sources 2006;156:321–33.

[2] Chan SH, Ho HK, Tian Y. Modeling of simple hybrid solid oxide fuel cell and gas turbine power plant. J Power Sources 2002;109:111–20.

[3] Naneda K, Mueller F, Brouwer J, Samuelsen S. Dynamic modeling and evaluation of solid oxide fuel cell-combined heat and power system operating strategies. J Power Sources 2010;195:3176–85.

[4] Meng GY, Jiang CR, Ma JJ, Ma QL, Liu XQ. Comparative study on the performance of a SDC-based SOFC fueled by ammonia and hydrogen. J Power Sources 2007;173:189–93.

[5] Zhu HY, Kee RJ, Pillai MR, Barnett SA. Modeling electrochemical partial oxidation of methane for cogeneration of electricity and syngas in solid oxide fuel cells. J Power Sources 2008;183:143–50.

[6] Klein JM, Bultel Y, Pons M, Ozil P. Modeling of a solid oxide fuel cell fueled by methane: analysis of carbon deposition. J Fuel Cell Sci Technol 2007;4:425–34.

[7] Huang K, Goodenough JB. Solid oxide fuel cell technology: principles, performance and operations. Cambridge [England]: Woodhead Publishing; 2009.

[8] Singhal SC, Kendall K. High temperature solid oxide fuel cells: fundamentals, design, and applications. New York, USA: Elsevier Science Publishers B.V.; 2003.

[9] Kreuer KD. Proton-conducting oxides. Annu Rev Mater Res 2003;33:333–59.

[10] Ni M, Leung DYC, Leung MKH. Mathematical modeling of ammonia-fed solid oxide fuel cells with different electrolytes. Int J Hydrogen Energy 2008;33:5765–72.

[11] Farhad S, Hamdullahpur F. Conceptual design of a novel ammonia-fuelled portable solid oxide fuel cell system. J Power Sources 2010;195:3084–90.

[12] Ma QL, Peng RR, Tian LZ, Meng GY. Direct utilization of ammonia in intermediate-temperature solid oxide fuel cells. Electrochem Commun 2006;8:1791–5.

[13] Bao C, Shi YX, Croiset E, Li C, Cai NS. A multi-level simulation platform of natural gas internal reforming solid oxide fuel cell – gas turbine hybrid generation system – part I. Solid oxide fuel cell model library. J Power Sources 2010;195:4871–92.

[14] Serincan MF, Pasaogullari U, Sammes NM. A transient analysis of a micro-tubular solid oxide fuel cell (SOFC). J Power Sources 2009;194:864–72.

[15] Suzuki M, Shikazono N, Fukagata K, Kasagi N. Numerical analysis of coupled transport and reaction phenomena in an anode-supported flat-tube solid oxide fuel cell. J Power Sources 2008;180:29–40.

[16] Li PW, Chyu MK. Simulation of the chemical/electrochemical reactions and heat/mass transfer for a tubular SOFC in a stack. J Power Sources 2003;124:487–98.

[17] Xue X, Tang J, Sammes N, Du Y. Dynamic modeling of single tubular SOFC combining heat/mass transfer and electrochemical reaction effects. J Power Sources 2005;142:211–22.

[18] Haberman BA, Young JB. A detailed three-dimensional simulation of an IP-SOFC stack. J Fuel Cell Sci Technol 2008;5:12.

[19] Ji Y, Yuan K, Chung JN, Chen YC. Effects of transport scale on heat/mass transfer and performance optimization for solid oxide fuel cells. J Power Sources 2006;161:380–91.

[20] Janardhanan VM, Deutschmann O. Numerical study of mass and heat transport in solid oxide fuel cells running on humidified methane. Chem Eng Sci 2007;62:5473–86.

[21] Iora P, Aguiar P, Adjiman CS, Brandon NP. Comparison of two IT DIR-SOFC models: impact of variable thermodynamic, physical, and flow properties. Steady state and dynamic analysis. Chem Eng Sci 2005;60:2963–75.

[22] Ferguson JR, Fiard JM, Herbin R. Three-dimensional numerical simulation for various geometries of solid oxide fuel cells. J Power Sources 1996;58:109–22.

[23] Yuan JL, Rokni M, Sunden B. Three-dimensional computational analysis of gas and heat transport phenomena in ducts relevant for anode-supported solid oxide fuel cells. Int J Heat Mass Transfer 2003;46:809–21.
[24] Ni M. Modeling of a planar solid oxide fuel cell based on proton-conducting electrolyte. Int J Energy Res 2010;34: 1027–41.
[25] Ni M, Leung DYC, Leung MKH. An improved electrochemical model for the NH_3 fed proton conducting solid oxide fuel cells at intermediate temperatures. J Power Sources 2008;185: 233–40.
[26] Chein RY, Chen YC, Chang CS, Chung JN. Numerical modeling of hydrogen production from ammonia decomposition for fuel cell applications. Int J Hydrogen Energy 2010;35:589–97.
[27] Yin SF, Xu BQ, Zhou XP, Au CT. A mini-review on ammonia decomposition catalysts for on-site generation of hydrogen for fuel cell applications. Appl Catal A: Gen 2004;277:1–9.
[28] Choudhary TV, Sivadinarayana C, Klinghoffer A, Goodman DW. Catalytic decomposition of methane: towards production of CO-free hydrogen for fuel cells. Stud Surf Sci Catal 2001;136:197–202.
[29] Zhang J, Xu HY, Jin XL, Ge QJ, Li WZ. Characterizations and activities of the nano-sized Ni/Al2O3 and Ni/La–Al2O3 catalysts for NH3 decomposition. Appl Catal A: Gen 2005;290: 87–96.
[30] Yin SF, Zhang QH, Xu BQ, Zhu WX, Ng CF, Au CT. Investigation on the catalysis of COx-free hydrogen generation from ammonia. J Catal 2004;224:384–96.
[31] Chellappa AS, Fischer CM, Thomson WJ. Ammonia decomposition kinetics over Ni-Pt/Al2O3 for PEM fuel cell applications. Appl Catal A: Gen 2002;227:231–40.
[32] Chase MW. NIST-JANAF thermochemical tables. 4th ed. American Chemical Society; American Institute of Physics for the National Institute of Standards and Technology; 1998.
[33] Wang CY. Fundamental models for fuel cell engineering. Chem Rev 2004;104:4727–65.
[34] Reid RC, Prausnitz JM, Polling BE. The properties of gases and liquids. 4th ed. McGraw-Hill Book Company, ISBN 0-07-051799-1; 1987.
[35] Yuan JL, Lv XR, Sunden B, Yue D. Analysis of parameter effects on transport phenomena in conjunction with chemical reactions in ducts relevant for methane reformers. Int J Hydrogen Energy 2007;32:3887–98.
[36] Chan SH, Khor KA, Xia ZT. A complete polarization model of a solid oxide fuel cell and its sensitivity to the change of cell component thickness. J Power Sources 2001;93:130–40.
[37] Demin AK, Tsiakaras PE, Sobyanin VA, Hramova SY. Thermodynamic analysis of a methane fed SOFC system based on a protonic conductor. Solid State Ionics 2002; 152-153:555–60.
[38] Patankar SV. Numerical heat transfer and fluid flow. New York: McGraw-Hill Book Company; 1980.
[39] Ni M. 2D thermal-fluid modeling and parametric analysis of a planar solid oxide fuel cell. Energy Convers Manag 2010;51: 714–21.
[40] Tseronis K, Kookos IK, Theodoropoulos C. Modeling mass transport in solid oxide fuel cell anodes: a case for a multidimensional dusty gas-based model. Chem Eng Sci 2008;63:5626–38.
[41] Lin Y, Ran R, Guo YM, Zhou W, Cai R, Wang J, et al. Proton-conducting fuel cells operating on hydrogen, ammonia, and hydrazine at intermediate temperature. Int J Hydrogen Energy 2010;35:2637–42.